Int. J. Electrochem. Sci., 7 **(2012)** 4974 - 4987

International Journal of
ELECTROCHEMICAL
SCIENCE
www.electrochemsci.org

Enhanced Electrocatalytic Performance for Methanol Oxidation via Insertion of Ruthenium Oxide Particles into Pt and Polyaniline-Poly(Acrylic Acid-co-Maleic Acid) Composite Electrode

Chung-Wen Kuo[1], *Zheng-Yan Kuo*[1], *Jiin-Jiang Jow*[1], *Tzi-Yi Wu*[2,*], *Jing-Yuan Chen*[2], *Xian-Xun Zhu*[2]

[1] Department of Chemical and Materials Engineering, National Kaohsiung University of Applied Sciences, Kaohsiung 80778, Taiwan, ROC
[2] Department of Chemical Engineering and Materials Engineering, National Yunlin University of Science and Technology, Yunlin 64002, Taiwan, ROC
[*]E-mail: wuty@yuntech.edu.tw

Received: 13 April 2012 / *Accepted:* 18 May 2012 / *Published:* 1 June 2012

Polyaniline (PANI) is doped with poly(acrylic acid-co-maleic acid) (PAMA) containing HCl to obtain PANI-PAMA film. Ultraviolet-visible spectroscopy results confirm the doping of PANI with PAMA and HCl. A scanning electron microscopy image reveals that the film is composed of highly porous nanowires. Platinum (Pt) particles are deposited into the PANI-PAMA film via electrochemical deposition to obtain PANI-PAMA-Pt composite electrodes. Subsequently, ruthenium oxide (RuO_2) particles are incorporated into the composite electrodes by cyclic voltammetry for 20 and 60 cycles to obtain PANI-PAMA-Pt-$RuO_2$20 and PANI-PAMA-Pt-$RuO_2$60 composite electrodes, respectively. The existence of RuO_2 particles is confirmed via characterization by X-ray photoelectron spectroscopy. X-ray diffraction analysis explains a decrease in the number of Pt crystalline facets for the incorporation of RuO_2 into PANI-PAMA-Pt, indicating a strong interaction between Pt and RuO_2. Cyclic voltammetry results and chronoamperometric response measurements demonstrate that the PANI-PAMA-Pt-$RuO_2$20 electrode has the best activity and stability toward methanol oxidation among the three electrodes.

Keywords: Polyaniline, poly(acrylic acid-co-maleic acid), nanowires, ruthenium oxide, cyclic voltammetry, methanol oxidation

1. INTRODUCTION

Fuel cells are regarded as promising devices for power generation and energy conversion [1-17]. Among the various types of fuel cell, direct methanol fuel cells (DMFCs) are highly attractive

power sources for a variety of applications due to their high energy efficiency, low emissions, low noise, and environmental friendliness [18-23]. However, DMFCs have two serious technical obstacles. A major problem associated with pure Pt catalysts is that they rapidly lose their activity due to the blockage of active sites by the adsorption of carbonaceous species produced in the electrooxidation of fuels. To alleviate this problem, Pt nanoparticles are usually alloyed with another metal, such as ruthenium (Ru) [24-26]. PtRu bimetallic catalysts are highly promising anode materials for DMFCs. The second metal (Ru) in these catalysts supplies OH-species at low potentials to remove poisoning CO species via the bifunctional mechanism [27]. The other issue for DMFCs is the slow kinetics of methanol oxidation on platinum. Accordingly, various Pt-based binary, ternary, and even quaternary compounds have been proposed to increase the catalytic activity of methanol oxidation [28-35]. In addition, the development of a supporting material is essential for minimizing noble metal loadings and achieving optimum catalytic performance. A promising strategy for the development of a supporting material is the introduction of conducting polymers (CPs) [36,37]. CPs have received increasing attention due to their potential applications in catalysis, nanotechnology, sensors, and microelectronics [38-41]. CPs are widely employed as porous supports on which electrocatalysts are dispersed and make low-loading catalysts feasible for fuel cell operation, lowering the cost of the system. Moreover, the interaction of the deposited Pt particles with the conducting polymer matrix favors the formation of OH species at a low positive potential, thus increasing the reaction rate of methanol oxidation [42].

CPs used as host matrices for the development of such systems are mainly polyaniline (PANI) [43,44], polypyrrole (PPy) [45,46], and polythiophene (PT) [47] by virtue of their excellent conducting properties and very good adhesion to the substrate electrode. Among these conducting polymers, PANI is the most widely studied due to its inherent characteristics of unique electronic properties, simple synthesis process, environmental stability, and low cost [48]. Recently, one-dimensional micro/nanostructured PANI has attracted interest as a potential building block for miniaturized nano-electronic devices [49] and highly sensitive (or biological) sensors [50,51]. Moreover, the introduction of PANI into the electrode catalyst layer increases Pt utilization, and thus less Pt is required.

Functionalized polymeric acids have been doped for PANI to increase its applicability. For instance, poly(styrenesulfonic acid) (PSS) has been shown to be easily incorporated in a CP matrix as a dopant of support for Pt particles. Huang *et al*. [52] reported that PANI-PSS acts as a matrix that leads to the uniform distribution of Pt particles. As a result, the electrocatalytic activity for methanol oxidation of PANI-PSS-Pt is much higher than that of PANI-Pt. Wen *et al.* [53] reported that highly dispersed Pt particles become homogeneously distributed in a poly(3,4-ethylenedioxythiophene)-poly(styrene sulfonic acid) (PEDOT-PSS) matrix. Kuo *et al.* [54] reported that PANI doped with poly(acrylic acid) (PAA) forms a spatial network structure. A PANI-PAA-Pt composite shows a significant enhancement of electroactivity for methanol oxidation. Accordingly, the incorporation of polymeric acids into PANI has been demonstrated to be an effective method for enhancing the electroactivity of electrodes.

In the present work, a polymeric acid poly(acrylic acid-co-maleic acid) (PAMA) containing HCl is employed as the dopant for PANI to form nanostructured PANI-PAMA film. Pt particles were deposited into the PANI-PAMA film via electrochemical deposition to obtain PANI-PAMA-Pt

composite electrodes. Then, RuO_2 particles were incorporated into the composite electrodes by cyclic voltammetry (CV) for 20 and 60 cycles to obtain PANI-PAMA-Pt-$RuO_2$20 and PANI-PAMA-Pt-$RuO_2$60 composite electrodes, respectively. The PANI-PAMA-Pt, PANI-PAMA-Pt-$RuO_2$20, and PANI-PAMA-Pt-$RuO_2$60 composite catalysts were characterized by X-ray photoelectron spectroscopy (XPS), X-ray diffraction (XRD), scanning electron microscopy (SEM), and energy-dispersive *X-ray* spectroscopy (*EDS*). The electrocatalytic activities of these composite catalysts were evaluated by CV and chronoamperometry methods. It is expected that Pt and RuO_2 particles deposited into PANI-PAMA film via electrochemical deposition can produce composite electrodes for use as a supporting material in DMFCs.

2. EXPERIMENTAL

2.1. Preparation of PANI-PAMA

A mixture solution of 0.1 M aniline (Merck) and 0.5 M H_2SO_4 (Merck) aqueous solutions was prepared. The electrochemical polymerization of the solution was carried out using the galvanostatic method with an indium-tin oxide (ITO) electrode as the working electrode for a charge of 0.1 C cm^{-2}, details of the procedure are described elsewhere [55]. Before each experiment, the ITO electrode was cleaned in an ultrasonic bath using detergent, deionized water, and isopropanol, and then dried in a nitrogen flow. The electrochemically deposited PANI-H_2SO_4 film was rinsed with double distilled water for 5 min and then dried at 120 °C for 3 min. The emeraldine base (EB) form of PANI was obtained by treating the PANI-H_2SO_4 film in 0.1 M ammonium hydroxide (Aldrich) for 3 min. The EB film was then redoped with 0.01 M PAMA (M_w = 3,000, Aldrich) and 0.01 M HCl. The EB film redoped with PAMA and HCl is denoted as PANI-PAMA.

2.2. Deposition of Pt and Pt-RuO_2 particles into PANI-PAMA matrixes

Pt particles were incorporated into PANI-PAMA film (PANI-PAMA-Pt) via electrochemical deposition from 0.01 M HCl + 0.1 M KCl solution containing 5 mM $H_2PtCl_6 \cdot 6H_2O$ with a constant deposition charge of 0.15 C at a constant potential of -0.2 V (vs. Ag/AgCl electrode). After Pt particle incorporation, RuO_2 particles were incorporated into PANI-PAMA-Pt film from 0.01 M HCl + 0.1 M KCl solution containing 5 mM $RuCl_3 \cdot 2H_2O$ by CV; the potentials were between 0.1 V and 0.8 V for 20 and 60 cycles (PANI-PAMA-Pt-$RuO_2$20 and PANI-PAMA-Pt-$RuO_2$60, respectively) with a scan rate of 10 mV sec^{-1}. After RuO_2 particle incorporation, the electrodes were rinsed with double distilled water for 5 min and then dried at 120 °C for 3 min. For comparison, RuO_2 particles were also deposited on a bare ITO electrode (E-RuO_2) using a similar method.

2.3. Physical and electrochemical characterizations

UV-Vis spectra of the PANI-H_2SO_4 (emeraldine salt), EB, and PANI-PAMA (emeraldine salt) films were recorded by a Perkin Elmer Lambda-35 UV-Vis spectrophotometer. An XPS study was

performed using an ESCA 210 spectrometer with Mg Kα ($h\nu$ = 1253.6 eV) irradiation as the photon source. The primary tension was 12 kV and the pressure during the scans was approximately 10^{-10} mbar. XRD patterns of the as-prepared electrodes were obtained by exposing the samples to a BRUKER D8 Discover SSS X-ray source with Cu Kα (λ = 0.154 nm) radiation as targets in the 2θ range of 10° to 80° with scan rate 4° min^{-1}. The surface morphologies of all electrodes were obtained using SEM (JEOL JSM-6700F) equipped with an energy-dispersive X-ray spectroscopy (EDS) detector.

Electrochemical characterizations of PANI-PAMA-Pt, PANI-PAMA-Pt-$RuO_2$20, and PANI-PAMA-Pt-$RuO_2$60 composite electrodes were carried out using a CHI627D electrochemical analyzer (U.S.A.). All experiments were performed in a three-component cell. An Ag/AgCl electrode (in 3 M KCl), a Pt wire, and an ITO electrode (1-cm^2 area) were used as the reference, counter, and working electrodes, respectively. A Luggin capillary, whose tip was set at a distance of 1-2 mm from the surface of the working electrode, was used to minimize errors due to the *iR* drop in the electrolytes.

2.4. Methanol electro-oxidation and stability of PANI-PAMA-Pt, PANI-PAMA-Pt-$RuO_2$20, and PANI-PAMA-Pt-$RuO_2$60 composite electrodes

The catalytic activities of PANI-PAMA-Pt, PANI-PAMA-Pt-$RuO_2$20, and PANI-PAMA-Pt-$RuO_2$60 composite electrodes were examined by CV at 10 mV sec^{-1} in the range of -0.2 to 1.2 V. Chronoamperometric response curves were obtained at 0.8 V in 1.0 M CH_3OH + 0.5 M H_2SO_4 solution. All the electrochemical experiments were carried out at room temperature.

3. RESULTS AND DISCUSSION

3.1. UV-Vis spectroscopy

The PANI-PAMA film was prepared via a doping-dedoping-redoping process, and was confirmed by UV-Vis spectroscopy results. Fig. 1 shows UV-Vis spectra for PANI doped form (electrochemical polymerization of PANI in H_2SO_4 medium), dedoped form, and redoped form with PAMA+HCl. The doped form of PANI (doped with H_2SO_4, curve *a*) has peaks at ca. 350 nm, 440 nm, and 850 nm (free carrier tail). These peaks correspond to electron transitions from the valance band to the polaronic band, which is characteristic of the doped emeraldine oxidation state of PANI [56]. Dipping the emeraldine salt of PANI with ammonium hydroxide yields the dedoped form of PANI. The corresponding UV-Vis spectrum (Fig. 1, curve *b*) exhibits absorption maxima at 330 nm and 630 nm, representing the π-π* transition and the charge transfer excitation-like transition bands, respectively, of the EB form of PANI [57]. The UV-Vis spectrum (Fig. 1, curve *c*) of the dedoped form of PANI in PAMA+HCl solution has three characteristic peaks and is similar to that of the PANI doped form (curve *a*). This indicates that PANI can be doped with PAMA+HCl via a simple doping-dedoping-redoping technique.

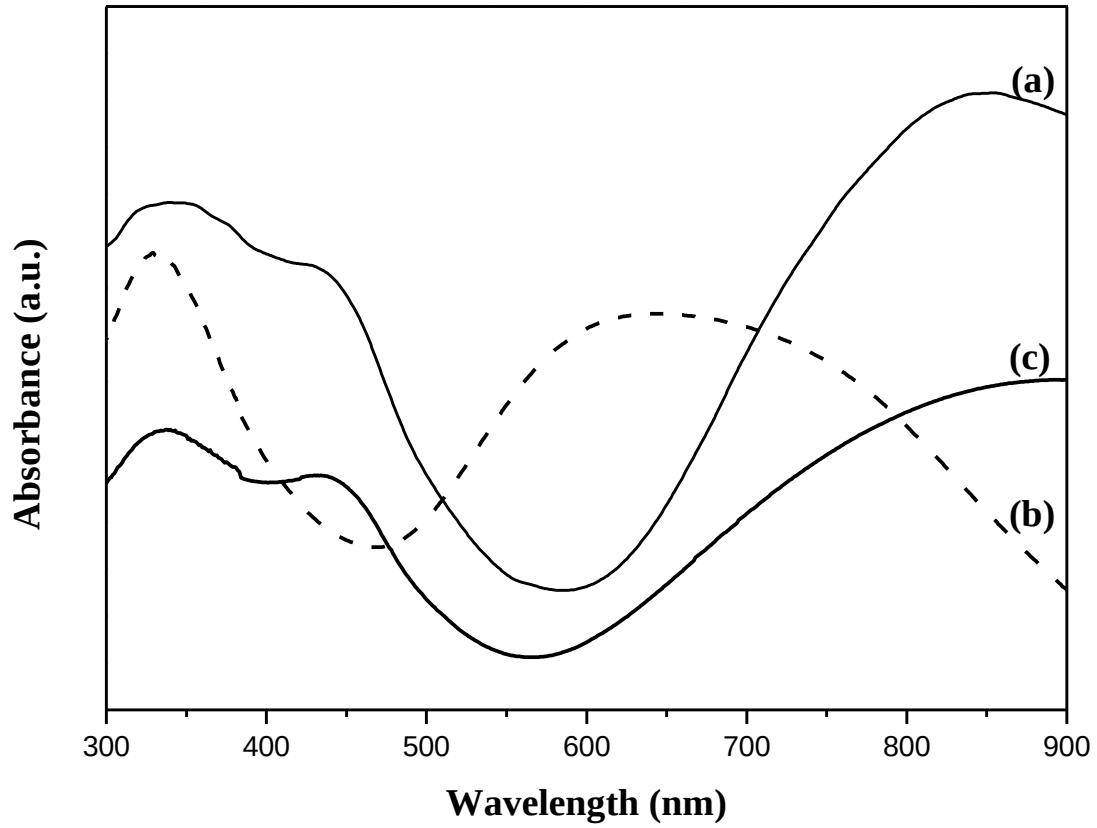

Figure 1. UV-Vis spectra of (a) PANI-H_2SO_4 (emeraldine salt), (b) emeraldine base (EB), and (c) redoped by PAMA+HCl (PANI-PAMA, emeraldine salt).

3.2. XPS analysis

Fig. 2a shows the survey scan of PANI-PAMA-Pt-$RuO_2$20. Signals due to C_{1s}, Cl_{2p}, N_{1s}, O_{1s}, Pt_{4f}, Ru_{3d}, and Ru_{3p} can be seen. The C_{1s} and Ru_{3d} signals of PANI-PAMA-Pt-$RuO_2$20 can be deconvoluted into four peaks (Fig. 2b). The peak at 284.6 eV comes from the carbon atoms of PANI. The C_{1s} peak at 287.7 eV can be assigned to carbon atoms functionalized by carboxyl groups of PAMA [58]. The XPS peak at 282.0 eV comes from the Ru $3d_{5/2}$ of RuO_2. The corresponding doublet Ru $3d_{3/2}$ signals can be deconvoluted into a peak at 285.2 eV. However, due to the overlapping of the Ru_{3d} with C_{1s} peaks, a clear determination of the ruthenium species was difficult, and thus the Ru_{3p} signal had to be used for the identification of Ru valence status (Fig. 2c). The peak of Ru_{3p} at 463.9 eV can be assigned to ruthenium(IV) oxide (RuO_2) [59]. These observations indicate the formation of RuO_2 in the PANI-PAMA-Pt-$RuO_2$20 electrode. The XPS analysis not only demonstrates the presence of elemental Pt and Ru but also shows that the Pt : Ru atomic ratio of composite electrodes. The Pt : Ru atomic ratio of PANI-PAMA-Pt-$RuO_2$20 and PANI-PAMA-Pt-$RuO_2$60 composite electrodes are 47:53 and 48:52, respectively.

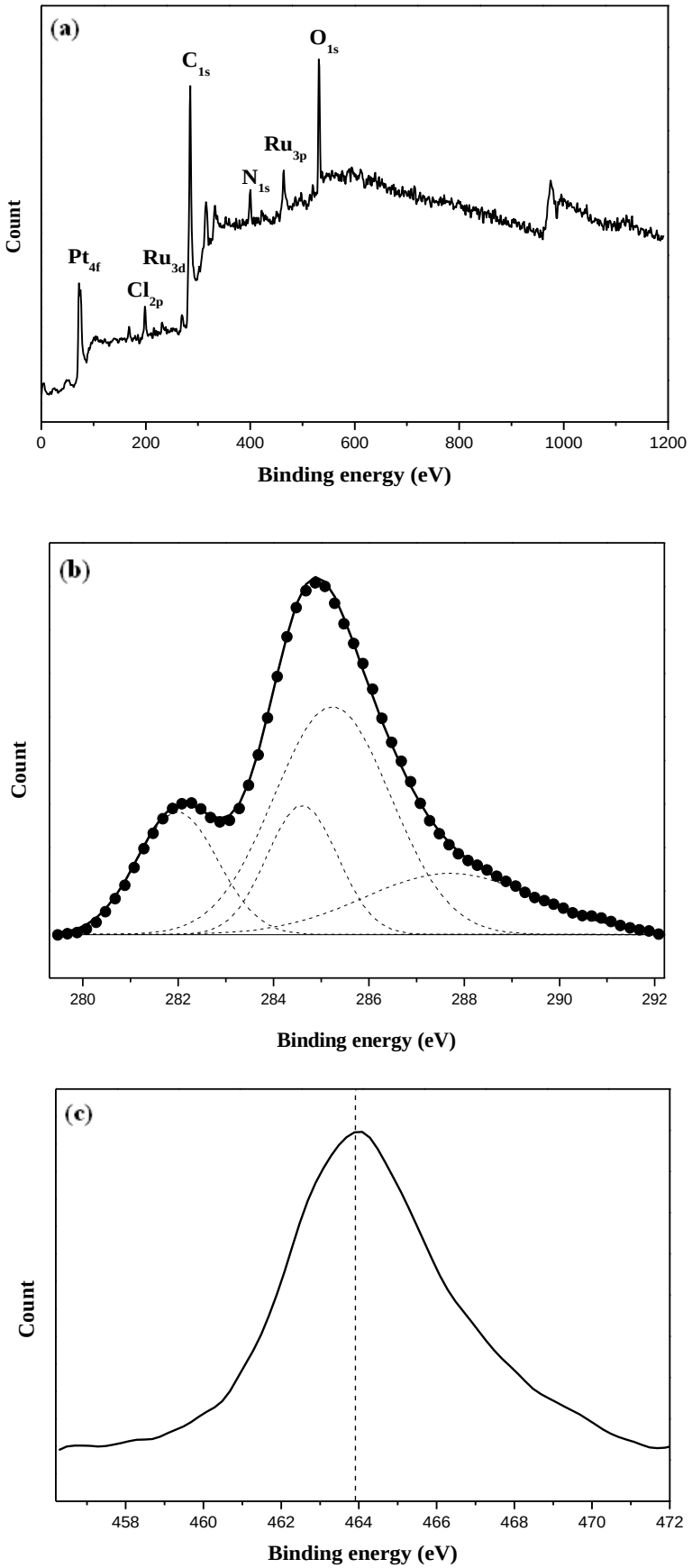

Figure 2. XPS spectra of (a) the survey scan, (b) Ru_{3d}/C_{1s} , and (c) Ru_{3p} for the PANI-PAMA-Pt $RuO_2$20.

Table 1. Atomic percentage of each element in PANI-PAMA-Pt, PANI-PAMA-Pt-$RuO_2$20, and PANI-PAMA-Pt-$RuO_2$60 electrodes from XPS analysis.

Electrode	C	N	O	Cl	K	Ru	Pt
PANI-PAMA-Pt	72.9	9.5	8.7	4.5	0.3	0.0	4.1
PANI-PAMA-Pt-$RuO_2$20	51.7	10.8	18.5	7.5	3.9	4.0	3.6
PANI-PAMA-Pt-$RuO_2$60	50.9	10.6	22.1	5.9	0.0	5.4	5.1

3.3. Structural characterization of composite electrodes

The nature of crystallinity of Pt and Pt-RuO_2 particles incorporated in a PANI-PAMA electrode was examined by XRD analysis; the results are shown in Fig. 3. The characteristic diffraction peaks of bare ITO appear at about 31°, 36°, 51°, and 61°, corresponding to the (222), (400), (440), and (622) planes, respectively [38]. Curve *a* in Fig. 3 shows the XRD pattern of PANI-PAMA-Pt. The characteristic diffraction peaks of face-centered cubic (fcc) platinum appear at 40°, 46°, and 68°, corresponding to the Pt (111), (200), and (220) planes, respectively. The diffraction peaks of RuO_2 were not found in the XRD pattern of PANI-PAMA-Pt-$RuO_2$20 and PANI-PAMA-Pt-$RuO_2$60 (Fig. 3, curves *b* and *c*) due to either the amorphous structure or low crystallinity of RuO_2. Comparing the half width of peaks, the Pt (111) and Pt (200) facets of PANI-PAMA-Pt-$RuO_2$20 and PANI-PAMA-Pt-$RuO_2$60 are broader than those of PANI-PAMA-Pt, as shown in the inset of Fig. 3. The reduced peak intensities of the Pt (111) and Pt (200) facets was observed for both PANI-PAMA-Pt-$RuO_2$20 and PANI-PAMA-Pt-$RuO_2$60, implying that the crystalline lattice of platinum might be influenced by the existence of RuO_2 particles in the composite system and the strong interaction between Pt and RuO_2.

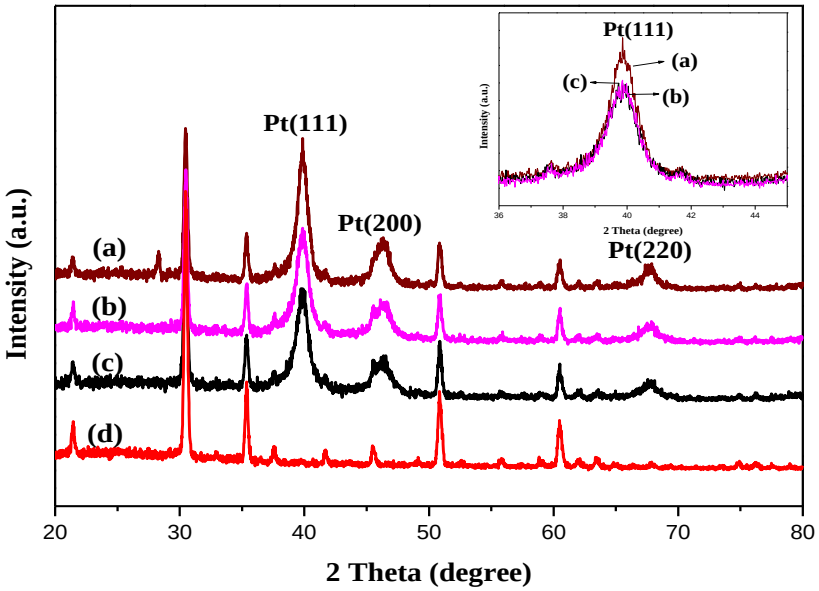

Figure 3. XRD patterns of (a) PANI-PAMA-Pt, (b) PANI-PAMA-Pt-$RuO_2$20, (c) PANI-PAMA-Pt-$RuO_2$60, and (d) PANI-PAMA.

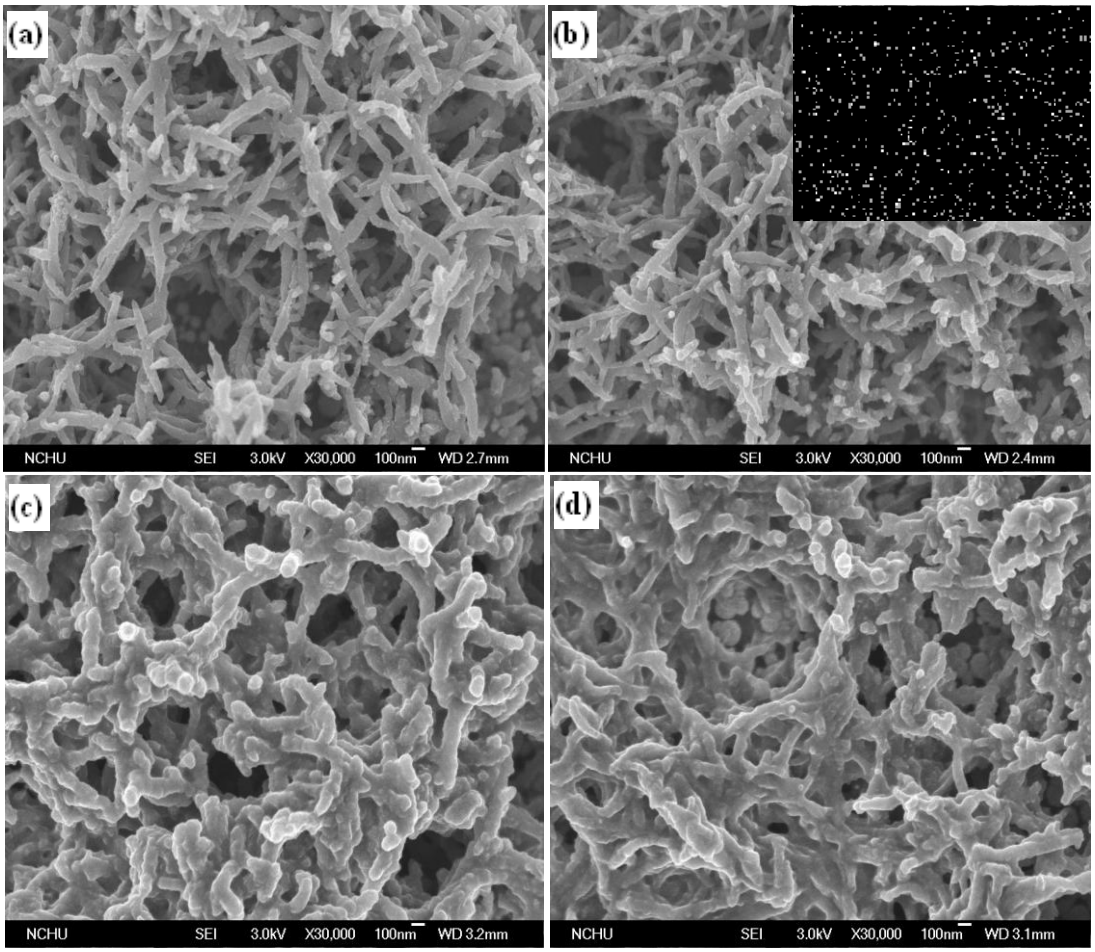

Figure 4. SEM images of (a) PANI-PAMA, (b) PANI-PAMA-Pt, (c) PANI-PAMA-Pt-$RuO_2$20, and (d) PANI-PAMA-Pt-$RuO_2$60. Inset of (b): X-Ray map shows bright spots for Pt.

3.4. Surface morphology of Pt and Pt-RuO_2 particles in PANI-PAMA film

Pt and Pt-RuO_2 catalysts supported on PANI-PAMA matrix were characterized by SEM and EDS analyses. Fig. 4a-d show SEM images of the surface morphology of PANI-PAMA, PANI-PAMA-Pt, PANI-PAMA-Pt-$RuO_2$20, and PANI-PAMA-Pt-$RuO_2$60 electrodes. The nanowire morphology of PANI-PAMA film can be seen in Fig. 4a. These nanowires have an average diameter of 50-90 nm. The nanowire morphology of this film provides a large surface area for the subsequent deposition of Pt particles. The Pt particles are believed to be incorporated into this nanowire network structure. The incorporation of Pt into PANI-PAMA (Fig. 4b) did not alter its morphology. Pt particles cannot be clearly seen in the SEM image of this composite electrode. Hence, particle mapping analysis was conducted to examine the surface morphology. The insets in Fig. 4b show EDS results of Pt in the composite electrode.

The bright spots indicate the existence of platinum in this electrode. The surface morphology of PANI-PAMA-Pt-$RuO_2$20 had a nanowire network structure with smaller pores, possibly due to the existence of a small amount of RuO_2 (Fig. 4c). The surface morphology of PANI-PAMA-Pt-$RuO_2$60 shows better cohesion with a compact layer structure, possibly due to the existence of a larger amount

of RuO_2 (Fig. 4d). The existence of RuO_2 cannot be seen in the SEM images of the two composite electrodes. Hence, the EDS plot confirms the existence of Pt and RuO_2 in the PANI-PAMA film (Fig. 5). The PANI-PAMA-Pt-$RuO_2$60 electrode contains more Ru and O atoms than that of PANI-PAMA-Pt-$RuO_2$20 due to the existence of a larger amount of RuO_2 (Table 1).

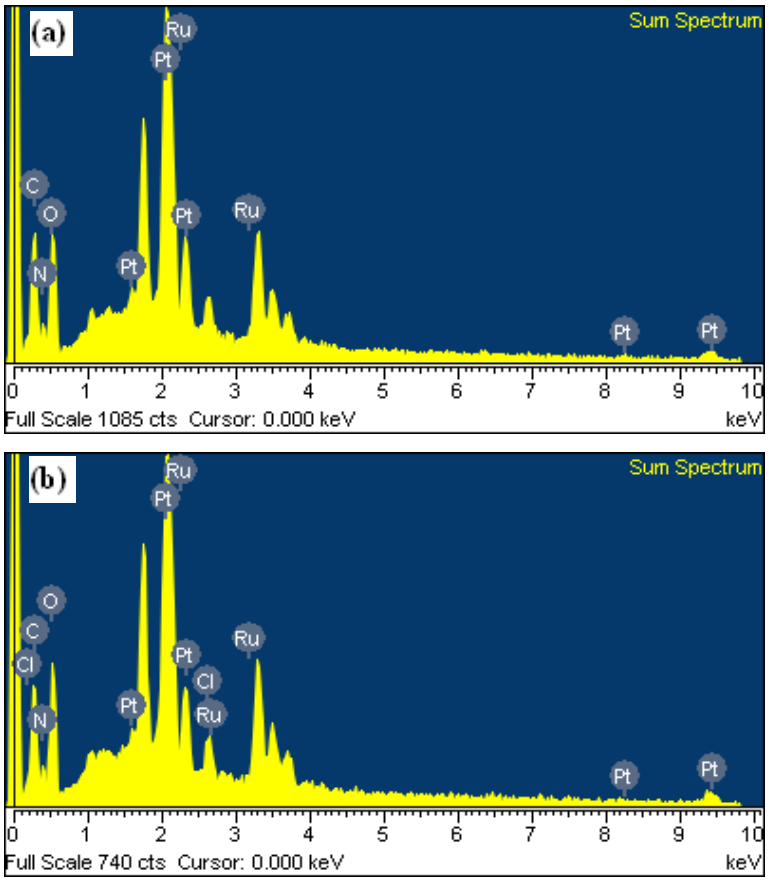

Figure 5. EDS plots for (a) PANI-PAMA-Pt-$RuO_2$20 and (b) PANI-PAMA-Pt-$RuO_2$60.

Schematic illustrations of the formation of PANI-PAMA-Pt-$RuO_2$20 and PANI-PAMA-Pt-$RuO_2$60 are showed in Fig. 6. The -CO_2H group in PANI-PAMA may act as a stabilizer for Pt particles, preventing their aggregation. Fig. 6a shows the spatial distribution of Pt particles in the polymer matrix PANI-PAMA.

A higher active surface area is expected with Pt particles dispersed in the PANI-PAMA matrix. After RuO_2 particle incorporation (20 cycles), homogeneous distributions of Pt and RuO_2 particles were obtained in the PANI-PAMA matrix. Moreover, larger aggregation was obtained with a higher number of cycles (60 cycles) in the deposition of RuO_2 particles (Fig. 6c), and the larger aggregation was homogeneously distributed in the PANI-PAMA matrix.

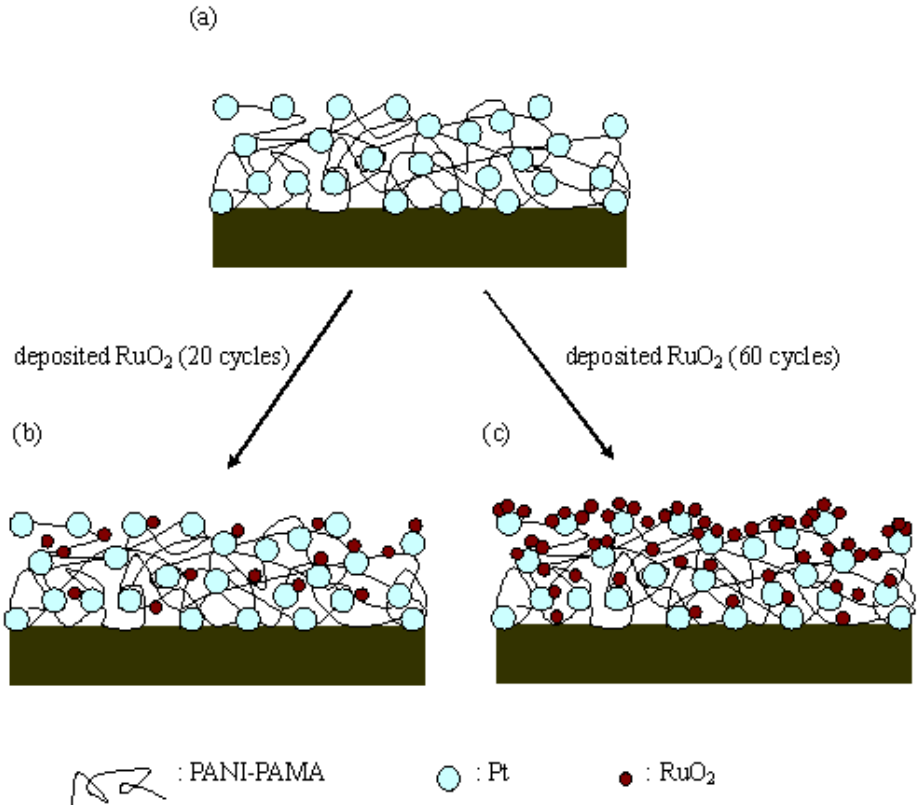

Figure 6. Schematic illustration for the formation of PANI-PAMA-Pt-$RuO_2$20 and PANI-PAMA-Pt-$RuO_2$60.

3.5. Electrocatalytic activity of Pt and Pt-RuO_2 particles loaded into PANI-PAMA film

Pt and Pt-RuO_2 particles were loaded into PANI-PAMA composite electrodes and tested for their electrocatalytic activity of methanol oxidation by cyclic voltammetry. Fig. 7 shows voltammograms of PANI-PAMA-Pt, PANI-PAMA-Pt-$RuO_2$20, PANI-PAMA-Pt-$RuO_2$60, and E-RuO_2 composite electrodes obtained in 0.5 M H_2SO_4 solution containing 1.0 M methanol at a scan rate of 10 mV s^{-1}. Comparing the CV results of the electrodes, a significantly higher oxidation current toward methanol oxidation was observed for PANI-PAMA-Pt-$RuO_2$20 compared to those of the other electrodes. A maximum anodic peak current density of 6.0 mA cm^{-2} was observed for the PANI-PAMA-Pt-$RuO_2$20 electrode (that for PANI-PAMA-Pt was 4.6 mA cm^{-2}). The voltammograms of the E-RuO_2 electrode show no characteristic methanol oxidation peak, indicating that E-RuO_2 particles are electro-catalytically inactive toward methanol oxidation (inset, Fig. 7d). The enhanced catalytic activity of PANI-PAMA-Pt-$RuO_2$20 toward methanol oxidation is thus attributed to the facile oxidation of methanol by RuO_2 particles in PANI-PAMA-Pt. However, the oxidation current density for methanol oxidation is about 3.2 mA cm^{-2} for PANI-PAMA-Pt-$RuO_2$60, which is lower than that of PANI-PAMA-Pt-$RuO_2$20. This might be due to an excessive number of RuO_2 particles covering the surface of Pt particles. In addition, the onset of methanol oxidation occurs at about 0.46, 0.40, and 0.41 V for PANI-PAMA-Pt, PANI-PAMA-Pt-$RuO_2$20, and PANI-PAMA-Pt-$RuO_2$60, respectively. The low onset of methanol oxidation observed in this study is due to less CO poisoning of Pt particles as a

result of the fast reaction between RuO_2 particles and the Pt-CO intermediate during methanol oxidation.

Based on the above supposition, the following mechanism is proposed for the oxidation of methanol in 0.5 M H_2SO_4 at the PANI-PAMA-Pt-$RuO_2$20 electrode by the dissociative adsorption process. This results in a series of adsorbed intermediates forming on the Pt surface [53,60].

$$CH_3OH+Pt \rightarrow Pt\text{-}(CH_ZO)_{ad}+(4\text{-}Z)H^+ +(4\text{-}Z)\, e^- \quad (0 \leq Z \leq 4) \ldots\ldots(1)$$

$$Pt\text{-}RuO_2 + H_2O \rightarrow Pt\text{-}RuO_2\,(OH) + H^+$$

The role of RuO_2 particles in platinum-RuO_2 catalysts for methanol oxidation is considered to be similar to that of ruthenium in platinum-ruthenium catalysts [61], in which species on ruthenium can oxidize the adsorption of CO on platinum. RuO_2 helps the transformation of adsorbed intermediates to carbon dioxide. The clean Pt surface then becomes available for further oxidation of methanol.

$$Pt\text{-}(CH_ZO)_{ad} + Pt\text{-}RuO_2\,(OH) \rightarrow Pt + Pt\text{-}RuO_2 + CO_2 + H_2O \ldots\ldots\ldots\ldots(2)$$

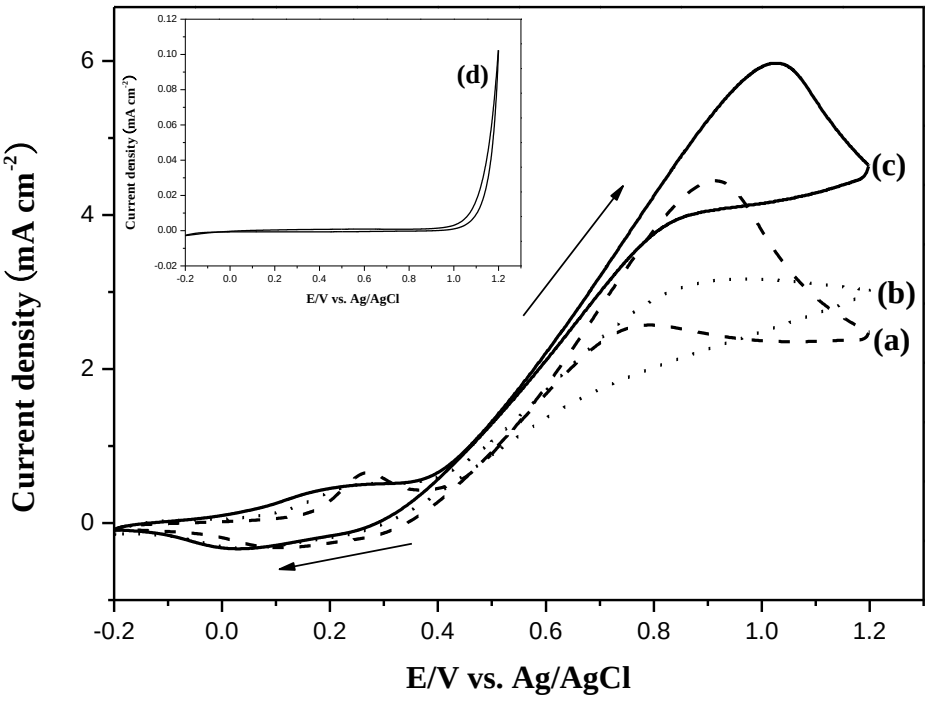

Figure 7. Cyclic voltammograms of (a) PANI-PAMA-Pt, (b) PANI-PAMA-Pt-$RuO_2$60, (c) PANI-PAMA-Pt-$RuO_2$20, and (d) E-RuO_2 (inset) in 1.0 M CH_3OH + 0.5 M H_2SO_4 solution with a scanning rate of 10 mV s^{-1}.

3.6. Electrocatalytic stability of Pt and Pt-RuO_2 particles loaded into PANI-PAMA film

Fig. 8 shows chronoamperometric responses for the oxidation of methanol at an applied potential of 0.80 V for PANI-PAMA-Pt, PANI-PAMA-Pt-$RuO_2$20, and PANI-PAMA-Pt-$RuO_2$60 in a solution of 0.5 M H_2SO_4 containing 1.0 M CH_3OH. It can be observed that PANI-PAMA-Pt-$RuO_2$20 electrocatalyst maintained the highest current density. For example, the currents at 300 s are 0.50, 0.30, and 0.15 mA cm^{-2} for PANI-PAMA-Pt-$RuO_2$20, PANI-PAMA-Pt-$RuO_2$60, and PANI-PAMA-Pt electrodes, respectively. Of note, these catalysts exhibit a current decay due to the formation of some Pt oxide or adsorbed intermediates during the methanol oxidation reaction [63].

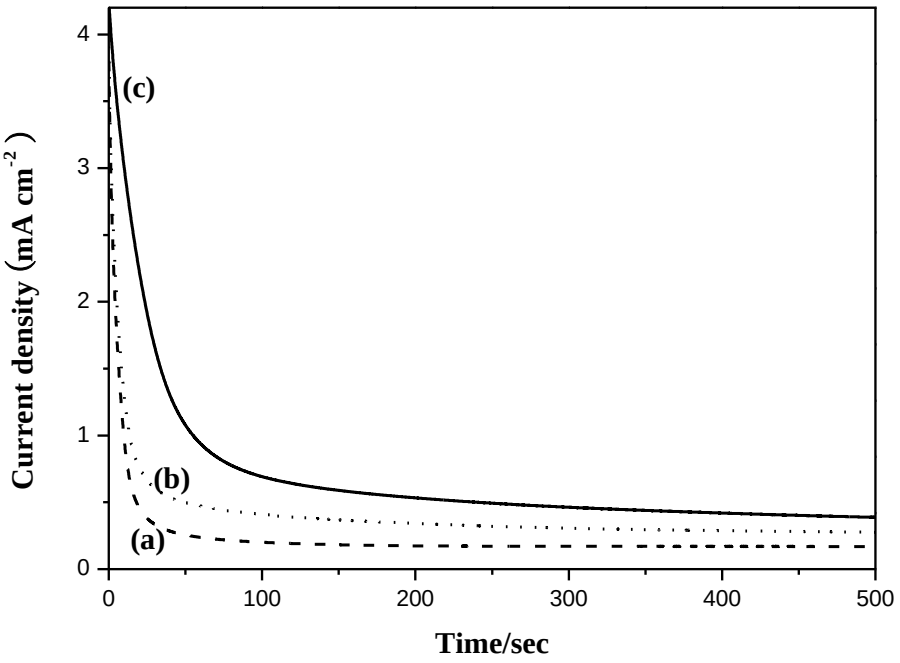

Figure 8. Chronoamperometric responses of (a) PANI-PAMA-Pt, (b) PANI-PAMA-Pt-$RuO_2$60, and (c) PANI-PAMA-Pt-$RuO_2$20 at 0.8 V (vs. Ag/AgCl) in 1.0 M CH_3OH + 0.5 M H_2SO_4 solution.

4. CONCLUSIONS

To fabricate an efficient electrode for methanol oxidation, PANI was doped with PAMA via a doping-dedoping-redoping process. The composite PANI-PAMA-Pt-$RuO_2$20-based electrode was demonstrated to be a promising material for methanol oxidation. The PANI-PAMA-Pt-$RuO_2$20 electrode exhibited the highest current density and stability toward methanol oxidation of the tested electrodes. The PANI-PAMA matrix provides an environment for dispersing Pt particles with low aggregation. RuO_2 favors the transformation of CO to carbon dioxide on a platinum surface. The -CO_2H group in the polymer matrix is interesting for 3D deposition of Pt and RuO_2, and the PANI-PAMA matrix is a potential candidate for preparing anode electrocatalysts for DMFCs.

ACKNOWLEDGEMENTS
The financial support of this work by the National Science Council of Taiwan under NSC 99-2218-E-151-003 is gratefully acknowledged.

References

1. B.C.H. Steele, A. Heinzel, *Nature*, 414 (2001) 345.
2. J. Gao, J. Liu, W. Liu, B. Li, Y. Xin, Y. Yin, Z. Zou, *Int. J. Electrochem. Sci.*, 6 (2011) 6115.
3. M.S. Mohy-Eldin, M.A. Abu-Saied, A.A. Elzatahry, K.M. El-Khatib, E.A. Hassan, M.M. El-Sabbah, *Int. J. Electrochem. Sci.*, 6 (2011) 5417.
4. R.S. Amin, A.A. Elzatahry, K.M. El-Khatib, M. Elsayed Youssef, *Int. J. Electrochem. Sci.*, 6 (2011) 4572.
5. H. Zhang, G. Lin, J. Chen, *Int. J. Electrochem. Sci.*, 6 (2011) 4714.
6. C. Guzmán, A. Alvarez, J. Ledesma-García, S.M. Duron-Torres, L.G. Arriaga, *Int. J. Electrochem. Sci.*, 6 (2011) 4787.
7. Y. Li, S.M. Chen, R. Sarawathi, *Int. J. Electrochem. Sci.*, 6 (2011) 3776.
8. J.H. Kim, S.K. Kim, Y.Z. You, D.I. Kim, S.T. Hong, H.C. Suh, K.S. Weil, *Int. J. Electrochem. Sci.*, 6 (2011) 4365.
9. A. Rezazadeh, A. Askarzadeh, M. Sedighizadeh, *Int. J. Electrochem. Sci.*, 6 (2011) 3105.
10. D.C. Huang, P.J. Yu, F.J. Liu, S.L. Huang, K.L. Hsueh, Y.C. Chen, C.H. Wu, W.C. Chang, F.H. Tsau, *Int. J. Electrochem. Sci.*, 6 (2011) 2551.
11. J.P. Spets, M.J. Lampinen, Y. Kiros, T. Anttila, J. Rantanen, T. Granström, *Int. J. Electrochem. Sci.*, 5 (2010) 547.
12. M. ELSayed Youssef, K.E. AL-NAdi, M.H. Khalil, *Int. J. Electrochem. Sci*., 5 (2010) 267.
13. C.M. Bautista-Rodríguez, M.G. A. Rosas-Paleta, J.A. Rivera-Marquez, N. Tepale-Ochoa, *Int. J. Electrochem. Sci.*, 6 (2011) 256.
14. A. Suzuki, T. Hattori, R. Miura, H. Tsuboi, N. Hatakeyama, H. Takaba, M.C. Williams, A. Miyamoto, *Int. J. Electrochem. Sci.*, 5 (2010) 1948.
15. M.B. Rodríguez, M.G.A.R. Paleta, J.A.R. Márquez, J.R.G. de la Vega, *Int. J. Electrochem. Sci*., 5 (2010) 414.
16. W.H. Chen, T.H. Ko, J.H. Lin, C.H. Liu, C.W. Shen, C.H. Wang, *Int. J. Electrochem. Sci.*, 6 (2011) 2192.
17. J.H. Myung, H.J. Ko, J.J. Lee, S.H. Hyun, *Int. J. Electrochem. Sci.*, 6 (2011) 1617.
18. A. Anis, S.M. Al-Zahrani, A.K. Banthia, S. Bandyopadhyay, *Int. J. Electrochem. Sci.*, 6 (2011) 2461.
19. A. Anis, S.M. Al-Zahrani, A.K. Banthia, S. Bandyopadhyay, *Int. J. Electrochem. Sci.*, 6 (2011) 2652.
20. H.D. Herrera-Méndez, P. Roquero, M.A. Smit, L.C. Ordóñez, *Int. J. Electrochem. Sci.*, 6 (2011) 4454.
21. H. Li, D. Kang, H. Wang, R. Wang, *Int. J. Electrochem. Sci.*, 6 (2011) 1058.
22. J. Parrondo, R. Santhanam, F. Mijangos, B. Rambabu, *Int. J. Electrochem. Sci.*, 5 (2010) 1342.
23. X.J. Feng , Y.L. Shi, Z.A. Hu, *Int. J. Electrochem. Sci.*, 5 (2010) 489.
24. R.M.S. Rodrigues, R.R. Dias, C.A.L.G.O. Forbicini, M. Linardi, E.V. Spinacé, A.O. Neto, *Int. J. Electrochem. Sci.*, 6 (2011) 5759.
25. A.B. Kashyout, A.A. Nassr Abu Bakr, L. Giorgi, T. Maiyalagan, B.A.B. Youssef, *Int. J. Electrochem. Sci.*, 6 (2011) 379.
26. R.M. Piasentin, E.V. Spinacé, M.M. Tusi, A.O. Neto, *Int. J. Electrochem. Sci.*, 6 (2011) 2255.
27. M. Watanabe, M. Uchida, S. Motoo, *J. Electroanal. Chem.*, 229 (1987) 395.
28. M. Brandalise, M.M. Tusi, R.M. Piasentin, M. Linardi, E.V. Spinace, A.O. Neto, *Int. J. Electrochem. Sci.*, 5 (2010) 39.

29. R.F.B. De Souza, M.M. Tusi, M. Brandalise, R.R. Dias, M. Linardi, E.V. Spinace, M.C. dos Santos, A.O. Neto, *Int. J. Electrochem. Sci.*, 5 (2010) 895.
30. M. Brandalise, M.M. Tusi, R.M.S. Rodrigues, E.V. Spinace, A.O. Neto, *Int. J. Electrochem. Sci.*, 5 (2010) 1879.
31. D. Morales-Acosta, D. López de la Fuente, L.G. Arriaga, G. Vargas Gutiérrez, F.J. Rodríguez Varela, *Int. J. Electrochem. Sci.*, 6 (2011) 1835.
32. D.F. da Silva, A.N. Geraldes, E.Z. Cardoso, M.M. Tusi, M. Linardi, E.V. Spinacé, A.O. Neto, *Int. J. Electrochem. Sci.*, 6 (2011) 3594.
33. R. Awasthi, R.N. Singh, *Int. J. Electrochem. Sci.*, 6 (2011) 4775.
34. G.S. Buzzo, M.J.B. Orlandi, E. Teixeira-Neto, H.B. Suffredini, *Int. J. Electrochem. Sci.*, 6 (2011) 3768.
35. C.H. Wan, J.M. Wei, M.T. Lin, C.H. Lin, *Int. J. Electrochem. Sci.*, 6 (2011) 889.
36. H.H. Zhou, S.Q. Jiao, J.H. Chen, W.Z. Wei, Y.F. Kuang, *J. Appl. Electrochem.*, 34 (2004) 455.
37. C.C. Yang, T.Y. Wu, H.R. Chen, T.H. Hsieh, K.S. Ho, C.W. Kuo, *Int. J. Electrochem. Sci.*, 6 (2011) 1642.
38. C.W. Kuo, C. Sivakumar, T.C. Wen, *J. Power Sources*, 185 (2008) 807.
39. T.Y. Wu, R.B. Sheu, Y. Chen, *Macromolecules*, 37 (2004) 725.
40. C.W. Kuo, T.C. Wen, *Eur. Polym. J.*, 44 (2008) 3393.
41. T.Y. Wu, Y. Chen, *J. Polym. Sci. A Polym. Chem.*, 42 (2004) 1272.
42. T. Frelink, W. Visscher, J.A.R. Veen, *J. Electroanal. Chem.*, 382 (1995) 65.
43. J. Yano, H. Hirayama, Y. Harima, A. Kitani, *J. Electrochem. Soc.*, 157 (2010) B506.
44. C.W. Kuo, B.K. Chen, Y.H. Tseng, T.H. Hsieh, K.S, Ho, T.Y. Wu, H.R. Chen, *J. Taiwan Inst. Chem. Eng.*, 2012, in press, doi: 10.1016/j.jtice.2012.03.008.
45. Y.C. Zhao, L. Zhan, J.N. Tian, S.L. Nie, Z. Ning, *Electrochim. Acta*, 56 (2011) 1967.
46. M.W. Martínez, T.T. Thompson, M.A. Smit, *Int. J. Electrochem. Sci.*, 5 (2010) 931.
47. V. Selvaraj, M. Alagar, I. Hamerton, *Appl. Catal. B Environ.*, 73 (2007) 172.
48. S.W. Ng, K.G. Neoh, J.T. Sampanthar, E.T. Kang, K.L. Tan, *J. Phys. Chem. B*, 105 (2001) 5618.
49. W.R. Salaneck, I. Lundstrom, W.S. Hang, A.G. MacDiarmid, *Synth. Met.*, 13 (1986) 291.
50. Y. Cao, P. Smith, A.J. Heeger, *Synth. Met.*, 48 (1992) 91.
51. Y. Hung, X. Duan, Y. Cui, L.J. Lauhon, K.H. Kim, C.M. Lieber, *Science*, 294 (2001) 1313.
52. L.M. Huang, W.R. Tang, T.C. Wen, *J. Power Sources*, 164 (2007) 519.
53. C.W. Kuo, L.M. Huang, T.C. Wen, A. Gopalan, *J. Power Sources*, 160 (2006) 65.
54. C.W. Kuo, C.C. Yang, T.Y. Wu, *Int. J. Electrochem. Sci.*, 6 (2011) 3196.
55. F.J. Liu, L.M. Huang, T.C. Wen, C.F. Li, S.L. Huang, A. Gopalan, *Synth. Met.*, 158 (2008) 767.
56. T.C. Wen, L.M. Huang, A. Gopalan, *Electrochim. Acta*, 46 (2001) 2463.
57. J. Huang, J.A. Moore, J.H. Acquaye, R.B. Kaner, *Macromolecules*, 38 (2005) 317.
58. H. Ago, T. Kugler, F. Cacialli, W.R. Salaneck, M.S.P. Shaffer, A.H. Windle, R.H. Friend, *J. Phys. Chem. B*, 103 (1999) 8116.
59. X. Fu, H. Yu, F. Peng, H. Wang, Y. Qian, *Applied Catalysis A: General*, 321 (2007) 190.
60. W. Li, J. Lu, J. Du, D. Lu, H. Chen, H. Li, Y. Wu, *Electrochem. Commun.*, 7 (2005) 406.
61. F.F. Ren, F.X. Jiang, Y.K. Du, P. Yang, C.Y. Wang, J.K. Xu, *Int. J. Electrochem. Sci.*, 6 (2011) 5701.
62. T.K. Chang, T.C. Wen, *Synth. Met.*, 158 (2008) 364.